Differential Loss of KIR4.1 Immunoreactivity in Multiple Sclerosis Lesions

Lucas Schirmer, MD,[1] Rajneesh Srivastava, MSc,[1] Sudhakar Reddy Kalluri, MSc,[1] Susanne Böttinger, MSc,[1] Marina Herwerth, MD,[1] Daniele Carassiti, PhD,[2] Barkha Srivastava, PhD,[3] Jens Gempt, MD,[4] Jürgen Schlegel, MD,[5] Tanja Kuhlmann, MD,[6] Thomas Korn, MD,[1,7] Richard Reynolds, PhD,[2] and Bernhard Hemmer, MD[1,7]

Objective: Serum antibodies against the glial potassium channel KIR4.1 are found in a subpopulation of multiple sclerosis (MS) patients. Little is known about the expression of KIR4.1 in human normal brain tissue and in MS lesions.
Methods: We analyzed the expression pattern of KIR4.1 in normal brain tissue and MS lesions of the subcortical white matter by immunohistochemistry. Markers of related glial proteins, myelin, and inflammatory cells were analyzed in parallel.
Results: KIR4.1 is expressed in oligodendrocytes and astrocytes in the adult human brain. In oligodendrocytes, KIR4.1 appears as a homotetramer channel, in astrocytes as homo- and heterotetramer channels together with KIR5.1. In acute MS lesions, KIR4.1 immunoreactivity (IR) was differentially lost on periplaque oligodendrocytes and perivascular astrocytes. In part of acute lesions, complement activation, apoptotic KIR4.1$^+$ glial cells, and phagocytes containing KIR4.1$^+$ fragments accompanied loss of glial KIR4.1 IR. Periplaque reactive astrocytes showed enhanced IR for both KIR4.1 and KIR5.1. In chronic active MS lesions, apart from a general loss of oligodendrocytes in the demyelinated area, we observed a decrease of astroglial KIR4.1 but not glial fibrillary acidic protein IR. In chronic inactive and remyelinating MS lesions, KIR4.1 IR was restored on astrocytes and found in a subset of presumably new myelinating oligodendrocytes.
Interpretation: The expression profile of KIR4.1 in glial cells and stage-dependent alterations of KIR4.1 IR in MS lesions are compatible with an immune response against KIR4.1 at least in a subset of MS patients.

ANN NEUROL 2014;75:810–828

Multiple sclerosis (MS) is a chronic inflammatory disease of the central nervous system (CNS). It is widely believed that the disease is caused by an autoimmune response targeting autoantigens expressed by oligodendrocytes.[1–3] Accordingly, MS lesions are characterized by inflammation, demyelination, and astrogliosis.[4–6]

We have recently identified autoantibodies against the glial adenosine triphosphate–sensitive inward rectifying potassium channel KIR4.1 (KCNJ10) in a subset of MS patients.[7] The antibodies bind to the first extracellular domain of KIR4.1 and might exert biological activity in vivo. In rodents, KIR4.1 is expressed by astrocytes and oligodendrocytes and is the main inward rectifying potassium channel and an important regulator of water and potassium homeostasis in the CNS.[8–15] KIR4.1 forms homotetrameric and heterotetrameric potassium channels together with KIR5.1 (KCNJ16).[13,16,17] Dysfunction or deletion of the *KIR4.1* gene in humans and mice is

View this article online at wileyonlinelibrary.com. DOI: 10.1002/ana.24168

Received May 6, 2013, and in revised form Apr 26, 2014. Accepted for publication Apr 26, 2014.

Address correspondence to Dr Hemmer, Department of Neurology, Klinikum rechts der Isar, Technische Universität München, Ismaninger Strasse 22, 81675 Munich, Germany. E-mail: hemmer@lrz.tu-muenchen.de

From the [1]Department of Neurology, Klinikum rechts der Isar, Technische Universität München, Munich, Germany; [2]Wolfson Neuroscience Laboratories, Division of Brain Sciences, Imperial College Faculty of Medicine, Hammersmith Hospital, London, United Kingdom; [3]Comprehensive Pneumology Center, Ludwig Maximilians University Munich and Helmholtz Center Munich, Munich, Germany; [4]Department of Neurosurgery, Klinikum rechts der Isar, Technische Universität München, Munich, Germany; [5]Division of Neuropathology, Institute of Pathology, Klinikum rechts der Isar, Technische Universität München, Munich, Germany; [6]Institute of Neuropathology, University Hospital Münster, Münster, Germany; and [7]Munich Cluster for Systems Neurology (SyNergy), Munich, Germany.

TABLE 1. Clinical and Pathological Characteristics of MS Patients (Snap-Frozen Autopsy Tissue)

Patient #	Age, yr	Sex	Disease Duration, yr	Disease Course	Death–Tissue Preservation Interval, hr	CSF and Tissue Antibody Titers, KIR4.1/AQP4 Protein ELISA		Staging of Subcortical White Matter Lesions and Lesion Distribution per MS Cases		
						Anti–KIR4.1-IgG, OD	Anti–AQP4-IgG, OD	Acute	Chronic Active	Chronic Inactive
1	71	F	35	SP	24	0.6793[a]	0.4594		2× PPWM, 2× DMWM	
2	42	F	6	PP	11	0.8664[a,b]	0.2090	2× PPWM, 2× DMWM		
3	53	M	11	SP	12	0.1913	0.0995	1× PPWM	1× DMWM	
4	34	F	11	SP	12	0.0833	0.1388	1× PPWM, 1× DMWM	3× PPWM, 3× DMWM	
5	51	F	23	SP	10	1.7118 (0.4068)[a,b]	0.3503 (0.0786)	1× PPWM	1× DMWM	
6	44	F	19	SP	20	0.9715	0.3628			2× PPWM, 2× DMWM
7	53	F	28	SP	17	0.6094	0.5516	1× PPWM		3× PPWM, 1× DMWM
8	53	M	16	SP	13	0.5265	0.1757			1× PPWM, 1× DMWM
9	42	F	19	SP	31	0.4086 (0.1131)	0.4418 (0.0977)			2× PPWM, 2× DMWM
10	57	F	19	SP	12	1.0136[a]	0.2263			3× PPWM, 2× DMWM
11	45	M	25	SP	24	n/a	n/a	1× PPWM, 1× DMWM	1× PPWM, 1× DMWM	
12	53	F	24	SP	21	2.6189[a,b]	0.4167	1× PPWM, 1× DMWM		1× RMWM,[c] 1× PPWM 1× DMWM
13	55	M	20	SP	19	1.5821[a]	0.3878	1× PPWM, 1× DMWM		1× PPWM, 1× DMWM

TABLE 1: Continued

Patient #	Age, yr	Sex	Disease Duration, yr	Disease Course	Death–Tissue Preservation Interval, hr	CSF and Tissue Antibody Titers, KIR4.1/AQP4 Protein ELISA		Staging of Subcortical White Matter Lesions and Lesion Distribution per MS Cases		
						Anti–KIR4.1-IgG, OD	Anti–AQP4-IgG, OD	Acute	Chronic Active	Chronic Inactive
14	51	M	2	PP	13	n/a	n/a		1× PPWM	
15	59	F	39	SP	21	2.1302 (0.3178)[a]	0.5508 (0.1235)		3× PPWM, 1× DMWM	4× RMWM[c]
16	35	F	5	SP	9	n/a	n/a	3× PPWM, 3× DMWM	1× DMWM	
17	45	F	16	SP	10	0.2322	0.1071		1× PPWM, 1× DMWM	
18	40	M	16	SP	27	0.8665[a,b]	0.3106	3× PPWM, 1× DMWM	2× PPWM, 4× DMWM	1× PPWM, 1× DMWM
19	50	F	23	SP	22	0.9589 (0.1578)[a,b]	0.1611 (0.0429)	1× PPWM, 1× DMWM	2× PPWM, 2× DMWM	
20	48	F	29	SP	21	1.6729[a]	0.6092			1× PPWM, 1× DMWM

Tissue antibody titers from selected cases are shown in parentheses.
[a]CSF samples that were considered to be anti-KIR4.1 positive.
[b]KIR4.1 antibody–positive CSF samples of cases with complement activation in histology.
[c]RMWM lesions are shown in Chronic Inactive column.
AQP4 = aquaporin-4; CSF = cerebrospinal fluid; DMWM = demyelinated white matter; ELISA = enzyme-linked immunosorbent assay; F = female; IgG = immunoglobulin G; M = male; MS = multiple sclerosis; n/a = not available; OD = optical density; PP = primary progressive MS; PPWM = periplaque white matter; RMWM = remyelinating white matter; SP = secondary progressive MS.

TABLE 2. Clinical and Pathological Characteristics of Control Patients (Snap-Frozen Autopsy Tissue)

Patient #	Age, yr	Sex	Cause of Death	Death–Tissue Preservation Interval, hr	CSF Antibody Titer, KIR4.1/AQP4 Protein ELISA	
					Anti–KIR4.1-IgG, OD	Anti–AQP4-IgG, OD
1	82	M	n/a	21	0.5423	0.3460
2	35	M	Carcinoma of the tongue	22	n/a	n/a
3	68	M	Cor pulmonale, heart failure	30	0.5690	0.1598
4	84	M	Carcinoma of the bladder	5	n/a	n/a
5	82	M	Myelodysplastic syndrome	21	0.4962	0.2346
6	70	M	Coronary heart disease	48	n/a	n/a
7	79	M	Myocardial infarction	20	n/a	n/a
8	50	M	Hodgkin lymphoma	45	n/a	n/a
9	62	F	Pulmonary embolism	48	n/a	n/a

AQP4 = aquaporin-4; CSF = cerebrospinal fluid; ELISA = enzyme-linked immunosorbent assay; F = female; IgG = immunoglobulin G; M = male; n/a = not available; OD = optical density.

associated with a severe dysmyelinating/demyelinating CNS phenotype, suggesting an essential role of the molecule for glial cell function.[9,12,18]

Neuropathological studies of MS lesions have strongly advanced our understanding of the pathogenic processes underlying lesion development in demyelinating diseases of

TABLE 3. Clinical and Pathological Characteristics of Biopsy Tissue from MS and Other Neurological Control Patients

Patient #	Age, yr	Sex	Pathological Characteristics	Underlying Disease; Clinical Features	Tissue Processing of Biopsy Material
1	58	F	Active MS lesion	Gd^+ WM lesion; multifocal Gd^- lesions	Snap frozen, formalin fixed, paraffin embedded
2	64	F	Active MS lesion	Gd^+ WM lesion	Snap frozen, formalin fixed, paraffin embedded
3	52	F	ADEM lesion	Widespread Gd^+ WM lesion	Snap frozen
4	41	M	PML lesion	HIV infection	Formalin fixed, paraffin embedded
5	70	M	PML lesion	Lymphoma	Formalin fixed, paraffin embedded
6	53	F	PML lesion	Lymphoma	Formalin fixed, paraffin embedded
7	59	M	PML lesion	Lymphoma	Formalin fixed, paraffin embedded
8	72	F	PML lesion	n/a	Formalin fixed, paraffin embedded
9	60	F	Glioma core and infiltration zone	Glioma WHO grade II	Snap frozen
10	67	F	Glioma core and infiltration zone	Glioma WHO grade IV	Snap frozen

CSF samples were not available.
ADEM = acute disseminated encephalomyelitis; F = female; Gd = gadolinium; HIV = human immunodeficiency virus; M = male; MS = multiple sclerosis; n/a = not available; PML = progressive multifocal leukoencephalopathy; WHO = World Health Organization; WM = white matter.

TABLE 4. Antibodies Used for Immunohistochemistry

Antigen	Clone	Dilution	Reference	Source
MOG	8–18C5	1:200	MAB5680	Merck Millipore, Billerica, MA
MOG	Z12	1:50	Magliozzi 2007[21]	S. Piddlesden, Cardiff, UK
MBP	Rabbit pc	1:500	A0623	DakoCytomation, Glostrup, Denmark
CNPase	SMI91	1:200	SMI91-R	Covance, Princeton, NJ
NogoA	11C7	1:3,000	Kuhlmann 2007[28]	M. Schwab, Zurich, Switzerland
Olig2	Rabbit pc	1:50	18953	IBL, Spring Lake Park, MN
Connexin-47 (Cx47)	4A11A2	1:200	37–4500	Invitrogen, Carlsbad, CA
MHC-II	LN3	1:50	ab49388	Abcam, Cambridge, UK
CD68	514H12	1:100	MCA1815	AbD Serotec, Puchheim, Germany
CD3	CD3–12 (rat)	1:100	MCA1477	AbD Serotec
C9neo	B7	1:50	Barnett 2009[34]	P. Morgan, Cardiff, UK
GFAP	2.2B10 (rat)	1:200	13–0300	Invitrogen
GFAP	6F2	1:100	M0761	DakoCytomation
ALDH1L1	ab56777	1:300	ab56777	Abcam
KIR4.1 (KCNJ10)	Rabbit pc	1:700 (TSA: 1:1,000)	APC-035	Alomone Labs, Jerusalem, Israel
KIR4.1 (KCNJ10)	1C11	1:100	WH0003766M1	Sigma-Aldrich, St Louis, MO
KIR5.1 (KCNJ16)	Rabbit pc	1:500	APC-123	Alomone Labs
Claudin-5 (Cldn5)	4C3C2	1:200	18–7364	Invitrogen
AQP4	Rabbit pc	1:400	AB3594	Merck Millipore

pc = polyclonal; TSA = tyramide signal amplification.

the CNS.[19–21] The discovery of autoantibodies against aquaporin-4 (AQP4) together with neuropathological studies of neuromyelitis optica (NMO) lesions helped to define this disease as an entity distinct from MS.[22–25] In acute NMO lesions, a loss of perivascular AQP4 immunoreactivity (IR) was observed. Of note, myelin fibers were relatively preserved despite astroglial loss of AQP4 IR.[24,25]

In the present study, we investigated KIR4.1 expression in normal brain tissue and subcortical MS white matter (WM) lesions. We observed expression of KIR4.1 predominantly in oligodendrocytes and a subset of astrocytes. KIR4.1 expression was lost in the center of acute and chronic active MS lesions but restored on astrocytes in chronic inactive lesions and re-expressed by oligodendrocytes in remyelinating lesions.

Materials and Methods

MS and Control Cases

We examined a total of 94 subcortical WM lesion areas from 31 snap-frozen corticosubcortical (leukocortical) tissue blocks obtained at autopsies from 14 female and 6 male MS patients (2 primary progressive MS, 18 secondary progressive MS) collected at the UK Multiple Sclerosis Tissue Bank, London, United Kingdom. The age of the MS patients ranged from 40 to 71 years (median = 51 ± 9 years), and the disease duration from 2 to 39 years (median = 19 ± 10 years; Table 1). Cerebrospinal fluid (CSF) specimens were available from 17 of 20 MS patients obtained at autopsy, with 10 cases showing a positive KIR4.1–immunoglobulin G (IgG) titer (cf Table 1). Serum samples were not available. Leukocortical snap-frozen control tissue comprising 9 subcortical WM areas was obtained together with 3 CSF samples from 9 autopsy cases (1 female and 8 male patients) without neurological disorders collected at the UK Multiple Sclerosis Tissue Bank and the Institute for Neuropathology, University of Münster, Münster, Germany (age range = 35–84 years; median = 70 ± 17 years; Table 2). MS autopsy cases and normal controls were supplemented by snap-frozen and paraffin-embedded biopsy material from 2 female patients with acute MS lesions (58 and 64 years old), 1 patient with an acute disseminated encephalomyelitis (ADEM) lesion (female; 52 years old), 5 patients with progressive multifocal leukoencephalopathy (PML) lesions (2 female and 3 male

patients; median 59 ± 11 years old), and 2 female glioma patients with specimens harboring both infiltration zone and glioma core tissue (60 and 67 years old; Table 3).

The study was carried out according to the applicable national ethical guidelines and legal regulations regarding the use of archival postmortem material. For diagnostic purposes, hematoxylin and eosin (HE) and Luxol fast blue/Periodic acid-Schiff (LFB/PAS) staining was used.

Immunohistochemistry

Immunohistochemistry was carried out on 10 and 20μm (confocal imaging) thick snap-frozen sections. In case of formalin-fixed and paraffin-embedded biopsy material, 4 to 5μm-thick sections were prepared. Snap-frozen sections were fixed with either 4% paraformaldehyde, ice-cold methanol, or ice-cold acetone. Paraffin-embedded sections were deparaffinized and hydrated, and antigen retrieval was achieved by heat (steamer)

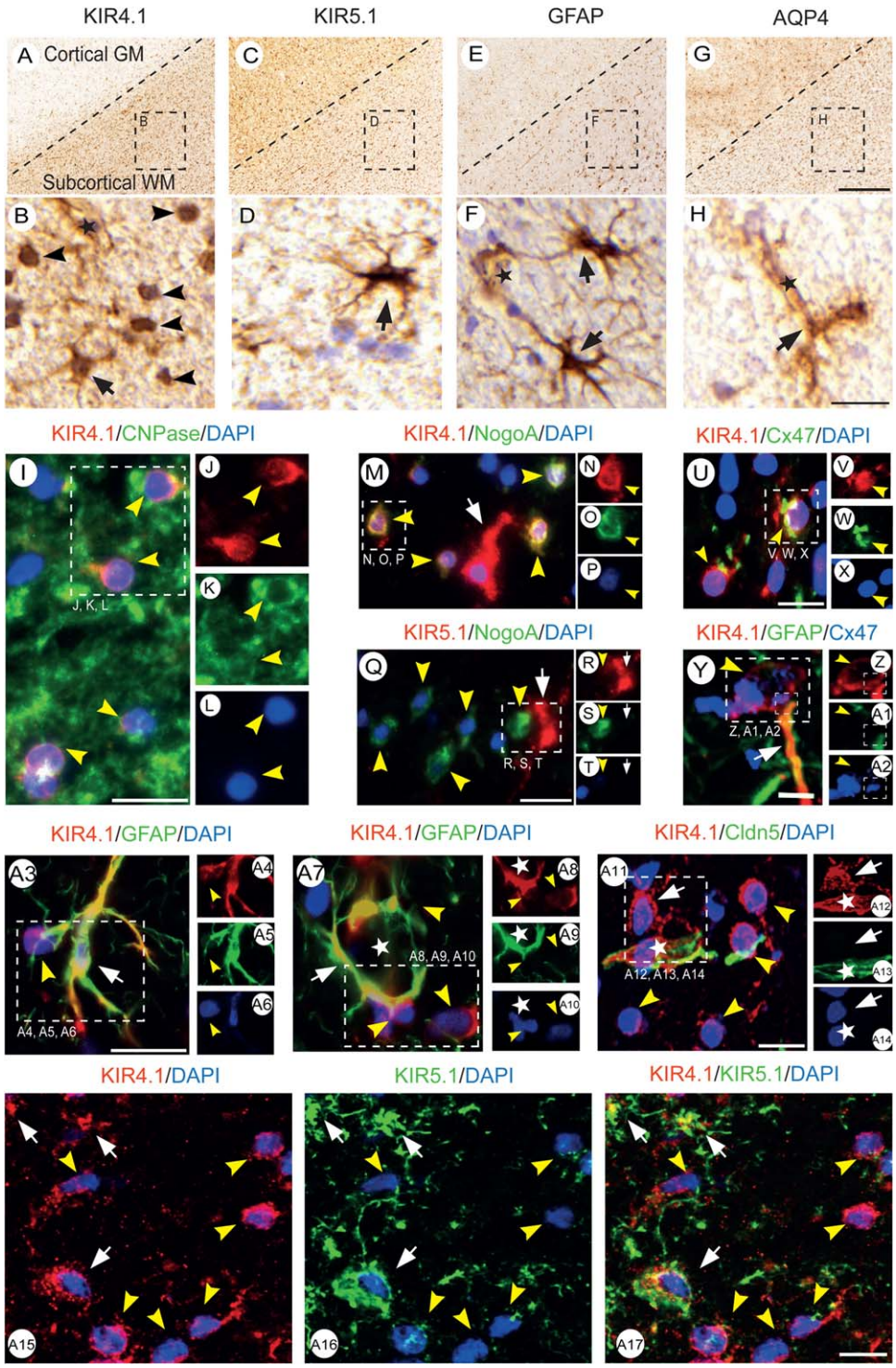

FIGURE 1.

in a 10mM citric buffer solution at pH 6. Subsequent blocking steps included peroxidase blocking with H_2O_2, avidin and biotin blocking (Vector Laboratories, Burlingame, CA), and normal serum blocking with 10% serum of species in which secondary antibodies were raised diluted in 1 × phosphate-buffered saline (PBS) supplemented with 0.1% Tween 20 (PBST). Incubations with primary antibodies (Table 4) diluted in PBST were carried out overnight at room temperature. Antibody detection was achieved using biotinylated secondary antisera (Vector) followed by avidin–peroxidase (Vectastain ABC; Vector). Diaminobenzidine (Invitrogen, Carlsbad, CA) and aminoethyl carbazole (Sigma-Aldrich, St Louis, MO) were used as chromogenic substrates. Negative control sections without primary antibodies were processed in parallel. Sections were counterstained with either hematoxylin, 4′,6-diamidino-2-phenylindole, or Hoechst nuclear counterstain (Invitrogen). Double and triple fluorescence staining using tyramide signal amplification of primary antibodies was conducted with fluorochromes tagged to streptavidin and secondary antibodies (Alexa Fluor 350, 488, and 555 dyes; Invitrogen). Terminal deoxynucleotide transferase–mediated deoxyuridine triphosphate nick-end labeling (TUNEL) was carried out according to the manufacturer's protocol (Invitrogen) and visualized by Alexa Fluor 488.

KIR4.1 Protein Enzyme-Linked Immunosorbent Assay and CSF KIR4.1-IgG Titers

For enzyme-linked immunosorbent assay (ELISA) of KIR4.1 reactivity in patients' CSF, protein oligomers were purified from HEK293 cells transfected with KIR4.1 or AQP4 cDNA, and affinity purification of the protein was performed as previously described.[7,26] Tetramers and higher-order oligomers were further purified using HiLoad16/600 Superdex 200 prep grade (GE Healthcare Bio-Sciences, Piscataway, NJ). We diluted KIR4.1 or AQP4 protein oligomers to 1μg/ml in PBS buffer and coated them on Nunc immobilizer amino plates (Thermo Scientific, Waltham, MA). Plates were blocked with blocking buffer (4% skimmed milk supplemented with 0.05% Tween 20 in PBS). CSF samples were diluted in 4% blocking buffer at a 1:2 ratio. We used an horseradish peroxidase–conjugated anti-human IgG antibody (Sigma) for detection. Optical density measurements were carried out at 450nm on a microplate reader (Tecan, Männedorf, Switzerland).

Positive KIR4.1-IgG titers in the CSF of MS patients were determined based on a cutoff value determined in control sera (0.53 ± 0.2; mean ± 5 SD; see Tables 1, 2). As further control, we analyzed anti-AQP4 CSF antibody titers from MS and control patients by the same method.

KIR4.1-IgG Isolation from MS Lesions

Isolation of total IgG from MS lesions was carried out according to a previously published protocol by O'Connor et al for isolation of myelin oligodendrocyte glycoprotein (MOG) antibodies from MS tissue.[27] For our purpose, we used 150mg of snap-frozen lesion tissue from 4 MS patients with different anti-KIR4.1 IgG titers in the CSF and harboring lesions of different inflammatory stage (MS #5, MS #9, MS #15, MS #19; cf Table 1). Isolated total IgG was then tested for reactivities against KIR4.1 and AQP4 by protein ELISA (see above).[7,26]

Microscopy and Image Analysis

Images were taken using a Zeiss Cell Observer microscope equipped with AxioCamICc 3 CCD and MRm cameras, and full section scans were taken by a Zeiss Mirax scanning system (Carl Zeiss Microimaging, Munich, Germany). Confocal images were taken using an Olympus FV1000 confocal microscope (Olympus Microscopy, Hamburg, Germany). Confocal image stacks were acquired sequentially. For confocal image representation, maximum intensity projections were generated using the freeware Fiji (http://rsbweb.nih.gov/ij). All images were processed to adjust irregularities in brightness and contrast using Photoshop software (Adobe Systems, San Jose, CA). Image panels were arranged and integrated into figures with Illustrator software (Adobe).

Statistical Analysis

Regarding postmortem MS tissue, we characterized 24 acute, 39 chronic active, 27 chronic inactive, and 5 remyelinating

FIGURE 1: Expression of KIR4.1 and related glial markers in normal human brain tissue. (A–H) Immunohistochemistry of the glial proteins KIR4.1 (A, B), KIR5.1 (C, D), GFAP (E, F),and AQP4 (G, H) in cortical gray matter and subcortical white matter (WM) of control tissue with staining of astrocytes *(black arrows)*, oligodendrocytes *(black arrowheads)*, and blood vessels (*black stars*; original magnification: A, C, E, G, ×50; B, D, F, H; ×400; scale bars: G, 500μm; H, 20μm. (I–L) Oligodendrocytes *(yellow arrowheads)* coexpressing KIR4.1 (red, J) and cyclic nucleotide phosphodiesterase (CNPase) in subcortical WM (green, K). (M–P) KIR4.1 (red, N) is colocalized with NogoA (green, O) on WM oligodendrocytes *(yellow arrowheads)*; (M) KIR4.1$^+$/NogoA$^-$ astrocyte is marked with white arrow. (Q–T) KIR5.1 (red, R) is not colocalized with NogoA$^+$ (green, S) on WM oligodendrocytes; KIR5.1$^+$/NogoA$^-$ astrocyte is marked with white arrow. (U–X) KIR4.1 (red, V) is colocalized with connexin-47 (Cx47)$^+$ (green, W) gap junctions on oligodendrocytes *(yellow arrowheads)*. (Y–A2) Confocal imaging of gap junction between oligodendrocyte *(yellow arrowhead)* and astrocytic process *(white arrow)* with KIR4.1 (red, Z), GFAP (green, A1), and Cx47 (blue, A2). (A3–A6) stellate WM astrocyte *(white arrow)* coexpressing KIR4.1 (red, A4) and GFAP (green, A5) adjacent to oligodendrocyte *(yellow arrowhead)*. (A7–A10) KIR4.1$^+$ (red, A8) and GFAP$^+$ (green, A9) astroglial ensheathing *(white arrow)* of small blood vessel *(white star)* adjacent to KIR4.1$^+$ oligodendrocytes (*yellow arrowheads*, A8). (A11–A14) Confocal imaging of blood vessel *(white star)* with KIR4.1 (red, A12) and claudin-5 (green, A13); yellow arrowheads indicate KIR4.1$^+$ glial cells of oligodendrocyte and white arrow of astrocyte morphology. (A15–A17) Confocal images of KIR4.1 (red, A15) and KIR5.1 (green, A16) double staining on human subcortical control tissue; astrocytes *(white arrows)* coexpress KIR4.1 and KIR5.1, and oligodendrocytes *(yellow arrowheads)* only express KIR4.1 but not KIR5.1 (merged, A17; original magnification: I, U, A3, A7, ×630; M, Q, ×400; Y, A11, A15–A17, ×600; scale bars: I, Q, U, A3, 20μm; Y, 3μm; A11, A17, 10μm). DAPI = 4′,6-diamidino-2-phenylindole.

WM lesion areas (see Table 1). Lesion areas were identified by MOG immunohistochemistry and LFB/PAS staining. With respect to WM lesion areas, we analyzed both lesion border (periplaque WM [PPWM]) and lesion core (demyelinated WM [DMWM]) separately. In PPWM and DMWM lesion areas, astroglial IR for KIR4.1 and glial fibrillary acidic protein (GFAP) was analyzed semiquantitatively in relation to the IR in corresponding control sections (0 = loss of IR, − = less than control level IR; −/+ = control level IR, + = more than control level IR, ++ = strongly enhanced IR). Prism software was used for graph generation (GraphPad Software, San Diego, CA).

Results

KIR4.1 Is Expressed by Oligodendrocytes and a Subset of Astrocytes in the Human Brain

We investigated the expression of KIR4.1 in human cortical gray matter (GM) and subcortical WM (Fig 1). Staining for KIR5.1, GFAP, and AQP4 served as

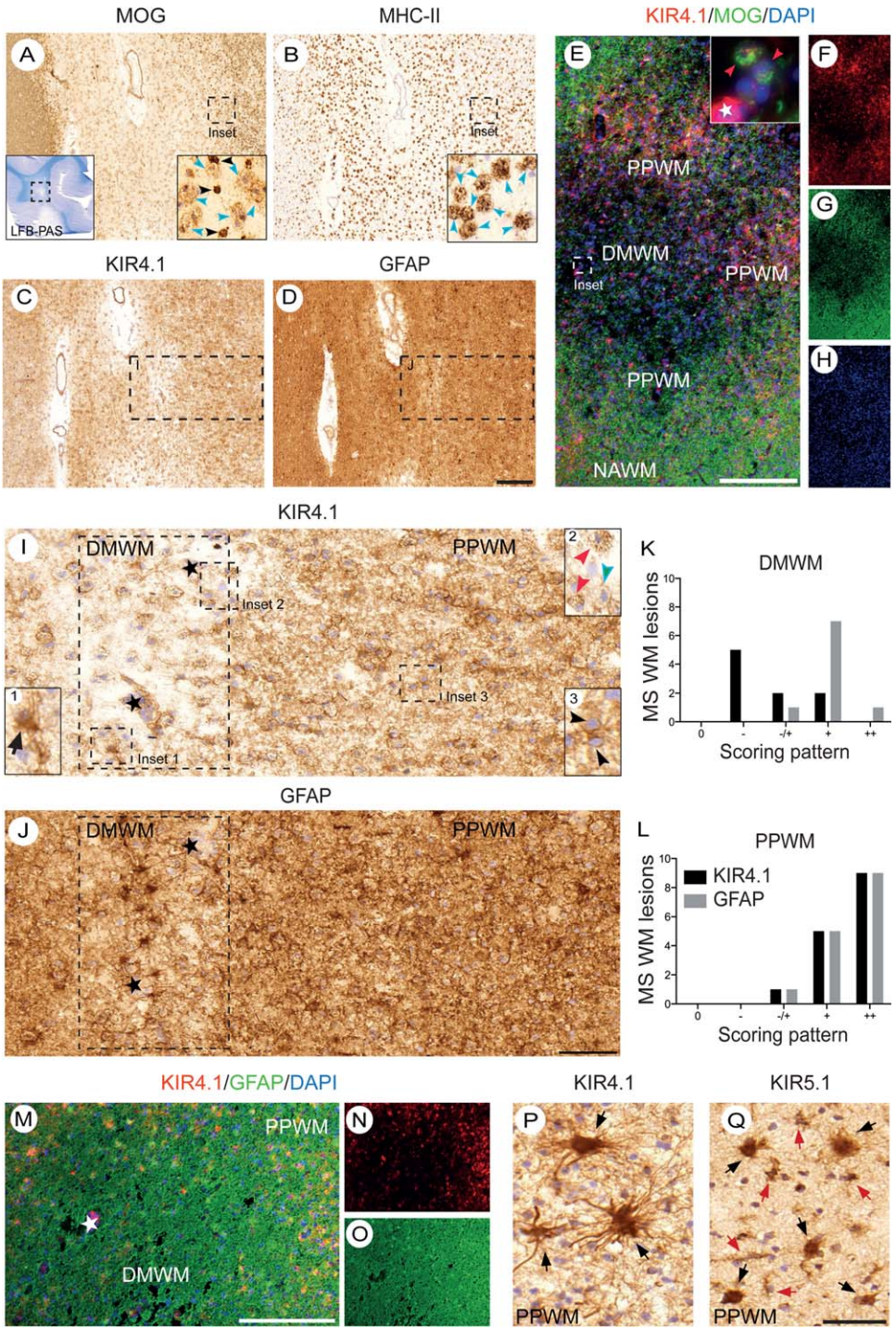

FIGURE 2.

controls. Expression of KIR4.1 was widely seen in cells with oligodendrocyte and astrocyte morphology in the subcortical WM. Double staining with cyclic nucleotide phosphodiesterase (CNPase) revealed that most of subcortical oligodendrocyte cell bodies expressed KIR4.1. Conversely, KIR4.1 was not found along $CNPase^+$ myelin sheaths. Additionally, KIR4.1 was colocalized with NogoA, suggesting that KIR4.1 is expressed in mature oligodendrocytes.[28] Of note, KIR5.1 was not found to be expressed in mature subcortical oligodendrocytes and thus was not colocalized with NogoA. The gap junction protein connexin-47 (Cx47) was associated with KIR4.1 on oligodendrocytes. Triple staining with KIR4.1, Cx47, and GFAP revealed that some $KIR4.1^+/GFAP^+$ astrocytic fibers were in contact with $KIR4.1^+$ cells of oligodendrocyte morphology at $Cx47^+$ membrane sites.[29] KIR4.1 was also expressed in a subset of fibrous stellate astrocytes in the subcortical WM and usually coexpressed with GFAP. Typically, astrocytic foot processes ensheathing blood vessels showed a high level of KIR4.1 expression.[13] Double staining with KIR4.1 and the endothelial tight junction protein claudin-5 (Cldn5) suggested that glial KIR4.1 is associated with the glia limitans of blood vessels. Furthermore, toward the meningeal surface, numerous astrocytes could be found with long $KIR4.1^+$ radial processes (data not shown). In the cortical GM, KIR4.1 was expressed at low levels in protoplasmic $ALDH1L1^+$ cell bodies in proximity to $KIR4.1^+$ cells of oligodendrocyte morphology (data not shown). Oligodendrocyte lineage of those cells in cortical GM was confirmed by costaining with KIR4.1 and both CNPase and NogoA (data not shown).

KIR4.1 appears in glial cells as homotetramers (homotetrameric KIR4.1) and heterotetramers with KIR5.1 (heterotetrameric KIR4.1) in cells that express both proteins.[13,16,17] Therefore, we stained human WM and GM brain tissue for KIR5.1. Expression of KIR5.1 was observed in astrocytes and a subset of cortical neurons (data not shown) but not in mature $NogoA^+$ oligodendrocytes (see Fig 1).[13,16,30] Moreover, KIR5.1 IR was not associated with Cldn5 (data not shown). Costaining for KIR4.1 and KIR5.1 confirmed absent KIR5.1 IR on cells of oligodendrocyte morphology.

In summary, mature oligodendrocytes express KIR4.1 but not KIR5.1 in the human brain. This suggests that only homotetrameric KIR4.1 channels occur in mature oligodendrocytes. By contrast, homotetrameric KIR4.1 and heterotetrameric KIR4.1/5.1 channels appear in the majority of WM astrocytes, which express both KIR4.1 and KIR5.1. Notably, perivascular astrocytic endfeet show strong KIR4.1 but not KIR5.1 staining.

Differential Loss of KIR4.1 IR on Oligodendrocytes and Astrocytes in Acute and Chronic Active Subcortical MS Lesions

Acute WM lesions displayed indistinct margins and were characterized by active demyelination in the lesion center with loss of MOG IR and presence of foam cells phagocytosing myelin fragments (MOG^+/LFB^+; Fig 2).[5,31–33] Furthermore, acute lesions typically exhibited extensive tissue infiltration with major histocompatibility complex (MHC)-II^+ phagocytes in both the lesion border and center. By double staining for MOG and KIR4.1, we observed a decrease of KIR4.1 IR in the lesion center (DMWM) with an upregulation in the PPWM, whereas the normal-appearing white matter (NAWM) showed a normal IR level as compared to control tissue.

FIGURE 2: Acute active demyelinating white matter (WM) lesions. (A) Immunohistochemistry for myelin oligodendrocyte glycoprotein (MOG; Luxol fast blue/Periodic acid-Schiff [LFB-PAS] staining shows section overview with active demyelinating WM lesion framed; *inset* in right corner demonstrates in higher magnification MOG^+ myelin fragments in foam cells *[cyan arrowheads]* adjacent to MOG^+ oligodendrocytes *[black arrowheads]*). (B) Major histocompatibility complex (MHC)-II immunohistochemistry of the same lesion as in A, showing strong infiltration of MHC-II^+ phagocytes (right *inset* demonstrates in higher magnification MHC-II^+ phagocytes at lesion border *[cyan arrowheads]*). (C) KIR4.1 and (D) glial fibrillary acidic protein (GFAP) immunoreactivity (IR) of the same lesion area shown in A and B demonstrates a perivascular loss of KIR4.1 but not GFAP IR. (E–H) Lesion overview shows normal-appearing WM (NAWM), periplaque WM (PPWM), and demyelinated WM (DMWM) lesion areas by costaining for KIR4.1 (red, F), and MOG (green, G); inset shows 2 foam cells (phagocytes) with MOG (green) and partially KIR4.1 (red) degradation fragments (white star marks blood vessel). (I) KIR4.1 and (J) GFAP IR of the framed lesion area in C and D demonstrates in higher magnification a differential loss of KIR4.1 but not GFAP IR in DMWM (framed); inset 1 shows a $KIR4.1^+$ reactive astrocyte, inset 2 displays 2 foam cells with incorporated KIR4.1 degradation products *(red arrowheads)* adjacent to foam cell (cyan arrowhead) without $KIR4.1^+$ debris, and inset 3 shows 2 $KIR4.1^+$ cells of oligodendrocyte morphology. (K, L) Summary of astroglial KIR4.1 and GFAP IR in active demyelinating lesions. Graphs show astroglial KIR4.1 and GFAP IR in 9 DMWM (K) and 15 acute PPWM (L) lesion areas (x-axis: 0 = loss of IR, − = less than control level IR; −/+ = control level IR, + = more than control level IR, ++ = strongly enhanced IR; y-axis: number of multiple sclerosis [MS] lesion areas). Note enhanced KIR4.1 and GFAP IR in PPWM areas due to reactive astrocytosis and differential loss of KIR4.1 but not GFAP IR in DMWM. (M–O) KIR4.1 (N) and GFAP (O) costaining (M, merged) showing differential loss of KIR4.1 IR in an acute perivascular lesion (vessel marked with *star*) with sustained astroglial GFAP IR in DMWM. (P, Q) Both cytoplasmic and fiber staining for KIR4.1 (P, homo- and heterotetrameric KIR4.1 channels) in reactive astrocytes *(black arrows)* in PPWM of active demyelinating lesion, but cytoplasmic only staining for KIR5.1 (Q, heterotetrameric KIR4.1 channels; note presence of $KIR5.1^+$ fibrous astrocytes adjacent to reactive astrocytes, *red arrows;* original magnification: A–D, I, J, ×50; E–H, M–O, ×10; P, Q, ×400; scale bars: D, M, 200μm; E, 500μm; J, 100μm; Q, 50μm). DAPI = 4′,6-diamidino-2-phenylindole.

Comparing KIR4.1 with GFAP staining, we noted a preferential perivascular loss of KIR4.1 but not of GFAP IR in active demyelinating WM lesions. Normally, perivascular astrocytic processes usually show a high KIR4.1 expression in control WM. Lesion borders were characterized by upregulation of KIR4.1 in reactive astrocytes. Notably, KIR4.1^{+} reactive astrocytes at lesion margins were characterized by the presence of both homo- and heterotetrameric KIR4.1 (IR for both KIR4.1 and KIR5.1).

Chronic active lesions displayed demarcated and hypercellular borders with a demyelinated lesion core, and were characterized by high densities of MHC-II^{+} macrophages and microglial cells at the lesion margins (PPWM; Fig 3).[5,32] Occasionally, PPWM phagocytes contained LFB^{+} but not MOG^{+} myelin fragments in

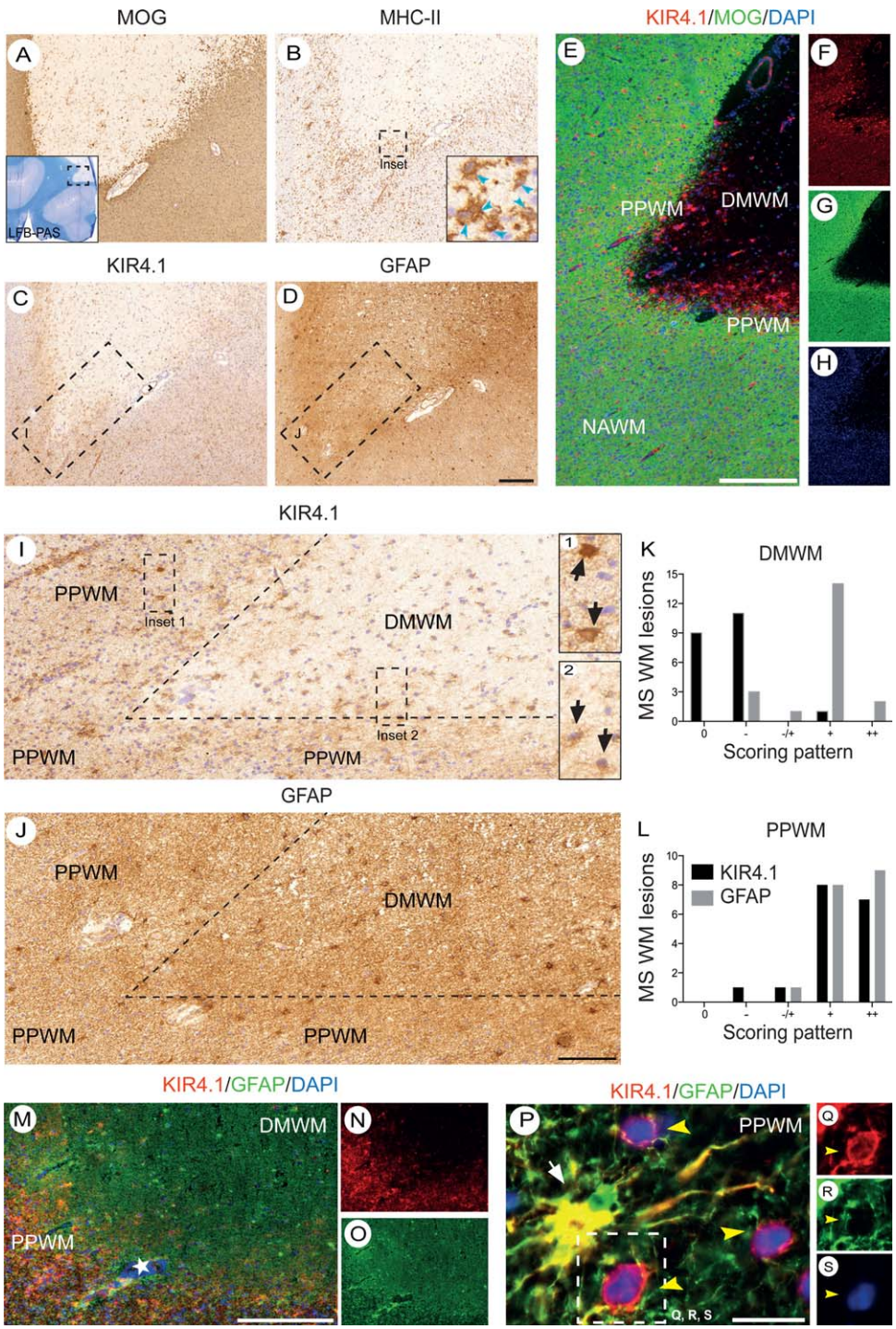

FIGURE 3.

the cytoplasm. Colabeling of KIR4.1 and MOG revealed a loss of KIR4.1 IR in the DMWM with an enhanced IR in the PPWM. Similar to active demyelinating lesions, we noted a substantial loss of KIR4.1 but not GFAP IR in DMWM chronic active lesion areas with an upregulation of KIR4.1 in PPWM reactive astrocytes. The differential loss of astroglial KIR4.1 with sustained GFAP IR was more pronounced in DMWM areas of chronic active lesions as compared with acute active demyelinating lesions. Reactive KIR4.1$^+$ astrocytes in PPWM areas of acute and chronic active lesions were identified by costaining with GFAP, and intermingled with remaining KIR4.1$^+$ oligodendrocytes.

To determine whether KIR4.1 IR was differentially lost on oligodendrocytes at lesion margins, we examined KIR4.1 and NogoA costaining in PPWM areas of 6 acute and chronic active lesions and 1 chronic inactive lesion (Fig 4). Additionally, we compared single stainings for MOG and KIR4.1 in PPWM areas of corresponding lesions. Accordingly, we noted a differential loss of KIR4.1 IR on NogoA$^+$ oligodendrocytes in parts of inflamed PPWM and adjacent DMWM areas of acute and chronic active lesions but not of chronic inactive lesion edges. In NAWM areas, KIR4.1 was consistently found to be colocalized with NogoA on oligodendrocytes. Similarly, some acute and chronic active PPWM areas exhibited preserved or new MOG$^+$ oligodendrocytes; however, an oligodendroglial KIR4.1 IR was mostly absent in those lesion areas.

These findings demonstrate a differential loss of KIR4.1 IR on a subset of oligodendrocytes in PPWM areas in at least part of the acute and chronic active MS lesions. Furthermore, a differential loss of KIR4.1 IR on astrocytes was observed in acute and chronic active MS lesions together with an upregulation of KIR4.1 and KIR5.1 in reactive astrocytes in the PPWM.

KIR4.1 Pathology Was Found to Be Associated with Active Phagocytosis, Complement Activation, and Cell Death

To determine whether KIR4.1 pathology was associated with active phagocytosis, complement activation, and cell death, KIR4.1 staining was combined with CD68 staining of phagocytes, C9neo staining visualizing complement activation, and TUNEL indicating DNA fragmentation. Accordingly, we found KIR4.1$^+$ glial cells with some of them showing oligodendrocyte morphology adjacent to CD68$^+$ phagocytes, and KIR4.1$^+$ degradation products within CD68$^+$ phagocytes (Fig 5; cf Fig 2E inset and 2I inset 2 for presence of KIR4.1$^+$ debris in cytoplasms of foam cells). Those acute MS lesions were characterized by perivascular cuffing and parenchymal infiltration of CD3$^+$ T cells. C9neo deposition was only found in 5 acute MS lesions in PPWM and active demyelinating DMWM lesion areas.[34] We also observed C9neo deposition on cells of oligodendrocyte morphology and the presence of C9neo-laden foam cells, partially in direct contact with KIR4.1$^+$ cells of oligodendrocyte morphology.[19,35] Of note, all lesions with C9neo deposition were obtained from MS patients with a positive anti-KIR4.1 CSF antibody titer. Notably, we could isolate IgG from tissue lysates obtained from 4 MS lesions of different lesion stages. Isolated IgG from patients with high CSF KIR4.1-IgG titers showed detectable antibody reactivity against KIR4.1 (MS cases #5 and #15) as compared to patients with low antibody titers in the CSF (MS cases #9 and #19; cf Table 1), demonstrating the presence of antibodies against KIR4.1 in selected acute and chronic active MS lesions. Notably, IgG reactivity against AQP4 was in all cases low and not increased in patients with higher tissue IgG reactivity against KIR4.1 (cf Table 1).

Combining KIR4.1 staining with TUNEL revealed the presence of KIR4.1$^+$ glial cells of oligodendrocyte

FIGURE 3: Chronic active demyelinated white matter (WM) lesions. (A) Myelin oligodendrocyte glycoprotein (MOG) immunohistochemistry (IHC; Luxol fast blue/Periodic acid-Schiff [LFB-PAS] staining shows section overview with chronic active demyelinated WM lesion framed). (B) Major histocompatibility complex (MHC)-II IHC of same lesion as in A showing strong infiltration of MHC-II$^+$ phagocytes and microglia at lesion border (right *inset* demonstrates in higher magnification MHC-II$^+$ phagocytes and microglia *[cyan arrowheads]*). (C) KIR4.1 and (D) glial fibrillary acidic protein (GFAP) immunoreactivity (IR) of the same lesion area shown in A and B demonstrates a substantial loss of KIR4.1 but not GFAP IR in demyelinated WM (DMWM). (E–H) Lesion overview shows normal-appearing WM (NAWM), periplaque WM (PPWM), and DMWM lesion areas by double staining for KIR4.1 (red, F), and MOG (green, G). (I) KIR4.1 and (J) GFAP IR of framed lesion area in C and D demonstrate in higher magnification a differential loss of KIR4.1 (I) but not GFAP (J) IR in DMWM (framed); insets 1 and 2 show KIR4.1$^+$ reactive astrocytes in PPWM. (K, L) Summary of astroglial KIR4.1 and GFAP IR in chronic active lesions: graphs show astroglial KIR4.1 and GFAP IR in 21 (n = 20 for GFAP) DMWM (K) and 18 (n = 17 for KIR4.1) PPWM (L) lesion areas (x-axis: 0 = loss of IR, − = less than control level IR; −/+ = control level IR, + = more than control level IR, ++ = strongly enhanced IR; y-axis: number of multiple sclerosis [MS] lesion areas). Note enhanced IR for KIR4.1 and GFAP in PPWM and differential loss of KIR4.1 but not GFAP IR in DMWM. (M–O) KIR4.1-GFAP costaining confirming differential loss of KIR4.1 IR (red, N) in a chronic active lesion with demarcated lesion border; note differential perivascular KIR4.1 IR loss around a vessel (marked with *star*) in the DMWM area. Note sustained astroglial GFAP IR (green, O) in DMWM. (P–S) KIR4.1 (red, Q) and GFAP (green, R) coexpressing reactive astrocyte *(white arrow)* in PPWM adjacent to KIR4.1$^+$ cells of oligodendrocyte morphology (*yellow arrowheads*; original magnification: A–D, I, J, ×50; E–H, M–O, ×10; P–S, ×630; scale bars: D, M, 200μm; E, 500μm; J, 100μm; P, 10μm). DAPI = 4′,6-diamidino-2-phenylindole.

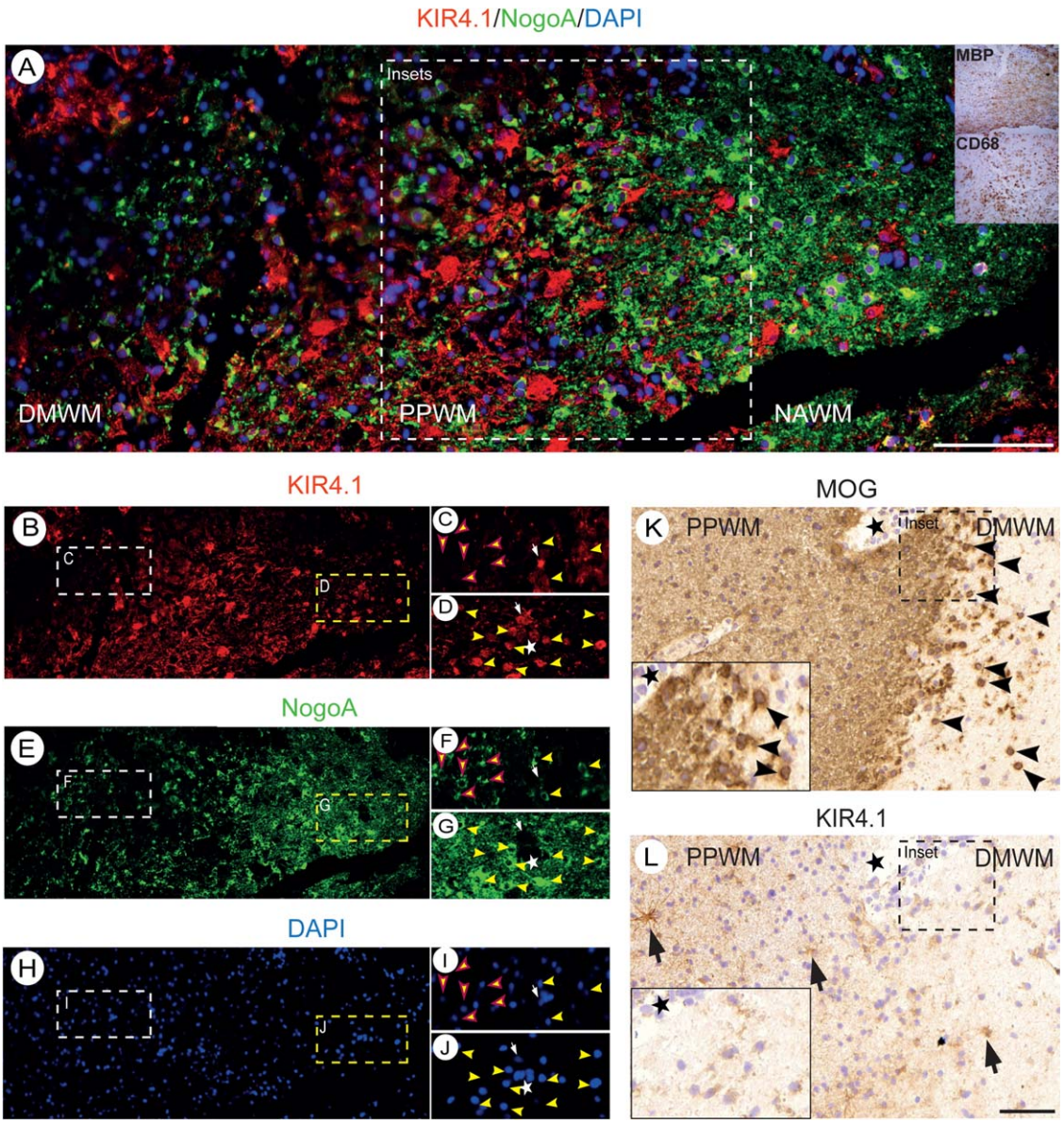

FIGURE 4: Differential oligodendroglial loss of KIR4.1 in acute and chronic active multiple sclerosis (MS) lesions. (A–J) KIR4.1 (red, A–D), NogoA (green, A, E–G), and 4′,6-diamidino-2-phenylindole (DAPI; A, H–J) staining of an acute MS lesion (right upper *insets* in A demonstrate lesion borders by myelin basic protein [MBP] immunohistochemistry [IHC] and infiltration of CD68$^+$ phagocytes); insets in B, E, and H (*left white inset,* demyelinated white matter [DMWM]; *right yellow inset,* normal-appearing white matter [NAWM]) are shown in higher magnification in C, F, and I (DMWM) and D, G, and J (NAWM). Note differential loss of KIR4.1 (red, C) but not NogoA (green, F) immunoreactivity (IR) on oligodendrocytes in DMWM (*yellow arrowheads with red outline,* KIR4.1 IR loss), whereas KIR4.1 (red, D) IR is preserved and colocalized with NogoA (green, G) on oligodendrocytes *(yellow arrowheads)* in NAWM. (K, L) Periplaque white matter (PPWM) of chronic active MS lesion with myelin oligodendrocyte glycoprotein (MOG; K) and KIR4.1 (L) IHC displays few preserved or new MOG$^+$ (K) oligodendrocytes in adjacent DMWM (*black arrowheads,* K; *inset* shows higher magnification), whereas KIR4.1 (L) IR is mostly lost on glial cells in corresponding DMWM (*black arrows* mark reactive KIR4.1$^+$ astrocytes in PPWM and DMWM areas; *black stars* mark vessel; original magnification: A, B, E, H, ×200; K, L, ×50; scale bars: A, L, 100μm).

morphology with TUNEL$^+$ nuclei indicating cell death in acute MS lesions (see Fig 5).

These findings demonstrate the occurrence of phagocytosis, T-cell infiltration, complement activation, and apoptosis of KIR4.1-expressing cells in acute MS lesions. Complement activation was only observed in patients with high CSF KIR4.1-IgG titers.

Regaining of KIR4.1 IR in Chronic Inactive Subcortical MS Lesions

Chronic inactive DMWM lesions were characterized by demarcated lesion edges with little or absent infiltration of macrophages and only little MHC-II$^+$ microglia activation in both the PPWM and DMWM (Fig 6).[5,32] In contrast to early stage lesions, we detected an enhanced

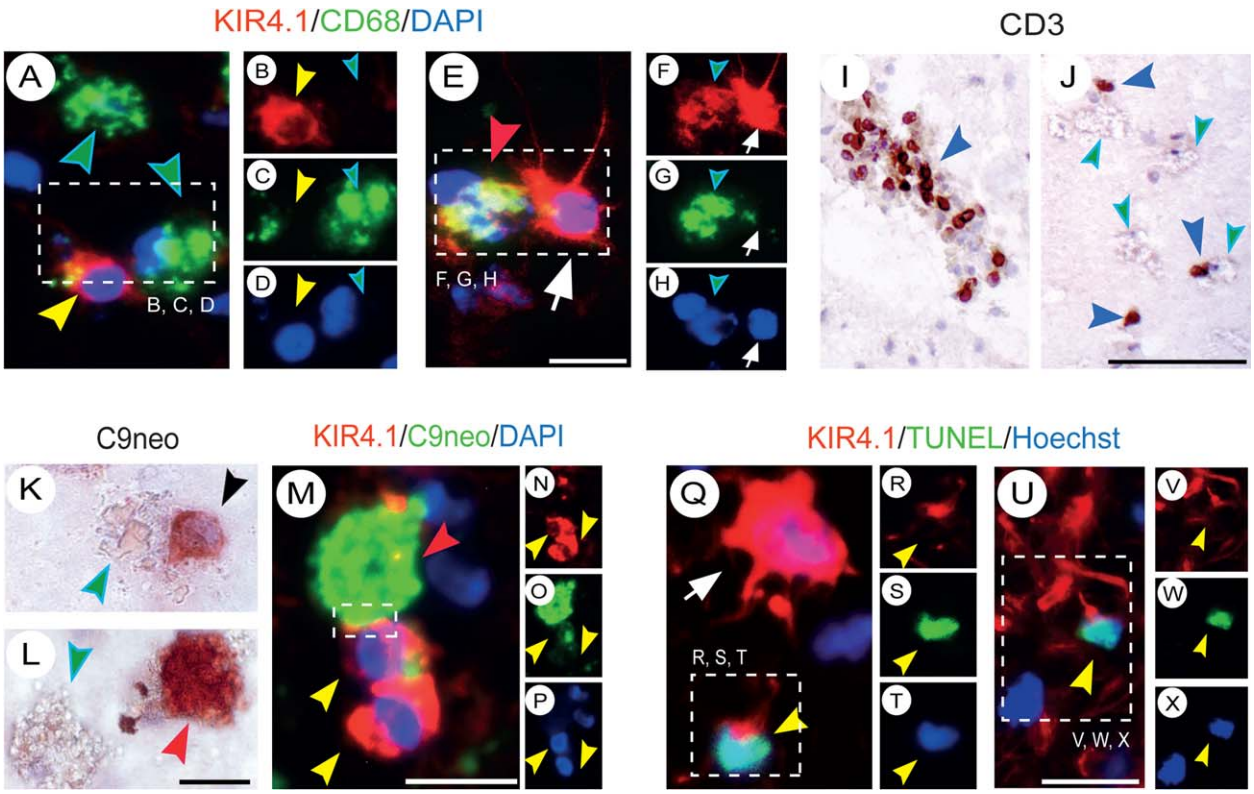

FIGURE 5: Acute multiple sclerosis (MS) lesions with evidence of KIR4.1-associated phagocytosis, complement activation, and cell death. (A–H) KIR4.1$^+$ glial cells with oligodendrocyte (red, A and B, *yellow arrowheads*) and astrocyte morphology (red, E and F, *white arrows*) attached to CD68$^+$ phagocytes (green, C, and G; *cyan arrowheads*) in acute demyelinated white matter with 1 CD68$^+$ phagocyte (E, framed) containing KIR4.1$^+$ fragments. (I, J) Perivascular cuffing (I) and parenchymal infiltration (J) of CD3$^+$ T cells *(blue arrowheads)* adjacent to foam cells *(cyan arrowheads)* in active demyelinating MS lesion. (K, L) C9neo deposition on cell of oligodendrocyte morphology (K, *black arrowhead*) in contact with foam cell *(cyan arrowhead)*, and C9neo-laden foam cell (L, *red arrowhead*; *cyan arrowhead* marks foam cells). (M–P) C9neo-laden foam cell (green, O; *red arrowhead*) in contact with KIR4.1$^+$ cells of oligodendrocyte morphology (red, N; *yellow arrowheads*). (Q–T) KIR4.1$^+$ (red, R) glial cell with oligodendrocyte morphology *(yellow arrowhead)* with nuclear terminal deoxynucleotide transferase–mediated deoxyuridine triphosphate nick-end labeling (TUNEL; green, S) in proximity to KIR4.1$^+$ reactive astrocyte (red, R; *white arrow* in Q). (U–X) Another example of KIR4.1$^+$ oligodendrocyte like cell with nuclear TUNEL (*yellow arrowhead;* original magnification: A, E, K, L, Q, U, ×630; I, J, ×200; M, ×400; scale bars: E, 10μm; J, 100μm; L, 10μm, M, 10μm; U, 20μm). DAPI = 4′,6-diamidino-2-phenylindole.

KIR4.1 IR in chronic demyelinated lesion areas. Regaining of KIR4.1 IR was paralleled by enhanced GFAP IR in DMWM areas. Astroglial KIR4.1 IR was confirmed by double staining for KIR4.1 and GFAP. Notably, in the chronic nonremyelinating DMWM, only few remaining CNPase$^+$ and MOG$^+$ (data not shown) myelin sheaths intermingled with KIR4.1$^+$ astrocytes and were found within a strong KIR4.1$^+$ astroglial fiber meshwork.

These results provide evidence that astroglial KIR4.1 IR is restored and increased along astrocytic fibers in chronic inactive DMWM lesions.

Regaining of Oligodendroglial KIR4.1 IR in Remyelinating MS Lesions

Remyelinating WM (RMWM) lesions were characterized by a sparse network of thin LFB$^+$ and MOG$^+$ myelin fibers (Fig 7). In RMWM areas, we observed a regaining of KIR4.1 IR on presumably new and mature oligodendrocytes as seen by double staining for KIR4.1 and NogoA. KIR4.1 staining combined with Olig2 immunohistochemistry revealed the presence of numerous Olig2$^+$ oligodendrocytes and precursor cells with a subset of those expressing KIR4.1. Staining of myelinating oligodendrocytes by Olig2 was confirmed by double staining with CNPase.

These findings demonstrate that KIR4.1 is expressed in remyelinating lesions in presumably new myelinating oligodendrocytes.

KIR4.1 Pathology in Other Neurological Diseases

To determine changes in KIR4.1 IR in other neurological diseases, we examined brain tissue harboring PML,

ADEM, and glioma lesions. Demyelinated PML lesions were characterized by loss of CNPase staining with a loss of NogoA$^+$/KIR4.1$^+$ oligodendrocytes (Fig 8 and data not shown) in the DMWM.[36,37] Conversely, the DMWM was characterized by a strong KIR4.1$^+$/GFAP$^+$ reactive astrogliosis. Regarding the PPWM, we detected an enhanced KIR4.1 IR in presumably JC virus–infected oligodendrocytes and astrocytes with enlarged nuclei. In perivascular ADEM lesions, we observed an enhanced KIR4.1 IR in reactive astrocytes with some preserved KIR4.1 staining on adjacent NogoA$^+$ oligodendrocytes in the PPWM.[38] In glioma infiltration zone tissue, we found KIR4.1 to be colocalized with NogoA on WM oligodendrocytes (data not shown) with a variable degree of KIR4.1$^+$ reactive astrogliosis toward the glioma core. Notably, in the glioma core we observed a strong KIR4.1

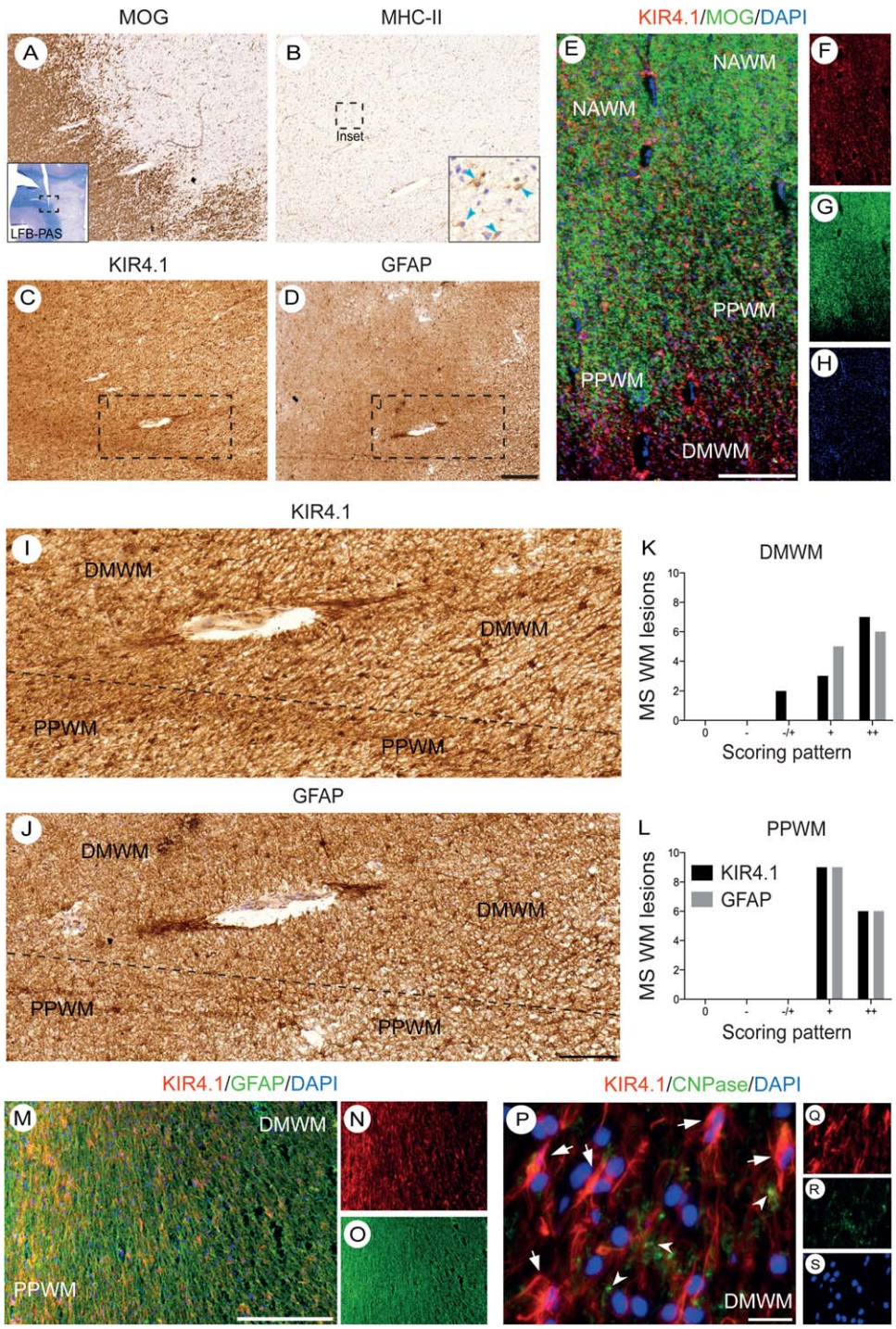

FIGURE 6.

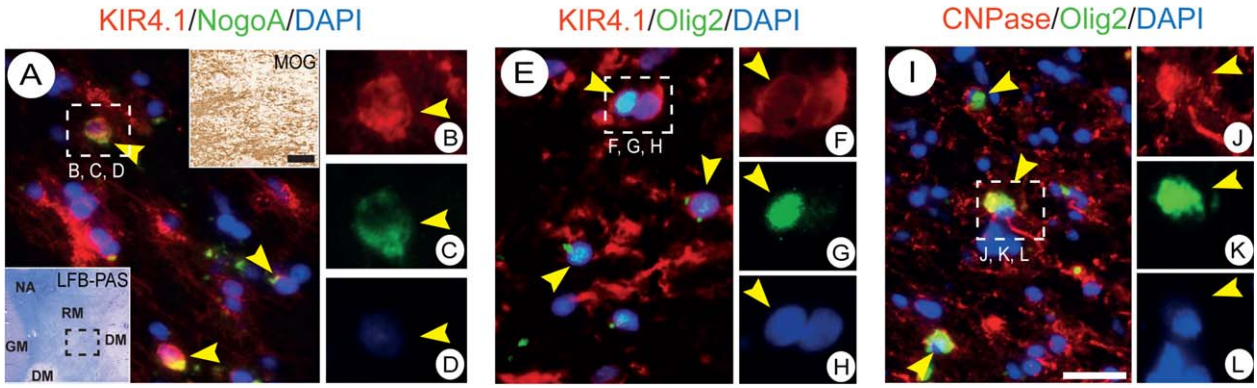

FIGURE 7: Remyelinating white matter (WM) lesions. (A–D) Regaining of KIR4.1 (red, B) immunoreactivity on NogoA$^+$ (green, C) oligodendrocytes in remyelinating WM (RMWM; *left inset* shows lesion overview with Luxol fast blue/Periodic acid-Schiff [LFB-PAS] staining; DM = WM demyelination; NA = normal-appearing WM; GM = normal-appearing gray matter; RM = white matter remyelination; *right inset* shows myelin oligodendrocyte glycoprotein [MOG] immunohistochemistry demonstrating sparse and thin MOG$^+$ myelin fibers in RMWM). (E–H) A subset of Olig2$^+$ (cyan nuclei, E; green, G) oligodendrocytes and precursor cells express KIR4.1 (red, F; Olig2$^+$/KIR4.1$^+$ oligodendrocytes = *yellow arrowheads* in E). (I–L) A subset of Olig2$^+$ (green, K) oligodendrocytes *(yellow arrowheads)* express cyclic nucleotide phosphodiesterase (CNPase; red, J; original magnification: A–L, ×630; A, right inset, ×100; scale bars: I, ×20μm; A, right inset, 200μm). DAPI = 4′,6-diamidino-2-phenylindole.

IR in glioma cells as seen with double staining for KIR4.1 and GFAP (data not shown).[39]

Overall, we found no evidence for a differential loss of KIR4.1 on oligodendrocytes and astrocytes in PML, ADEM, and glioma lesions.

Discussion

We previously identified serum autoantibodies against the inward rectifying potassium channel KIR4.1 in a subset of MS patients with demyelinating diseases of the CNS.[7,26] Although KIR4.1 antibodies are only rarely found in patients with other neurological diseases or healthy donors, it remains to be determined whether the occurrence is indicative of a primary immune response to KIR4.1 or a secondary phenomenon following CNS inflammation that is driven by autoimmune responses toward other autoantigens. In this context, pathological studies have greatly contributed to the understanding of the role of AQP4 in NMO.[24,25,40] Here, we analyzed the expression of KIR4.1 in the adult human brain and during the development of MS lesions as compared with other neuropathological conditions (PML, ADEM, and glioma).

We found that KIR4.1 is predominantly expressed by oligodendrocytes and a subset of astrocytes. Our data suggest that mature oligodendrocytes express KIR4.1 homotetrameric complexes, whereas astrocytes express both homo- and heterotetrameric KIR4.1/5.1 complexes.[13] Based on previous reports and our confocal costaining with Cx47, we conclude that KIR4.1 is located in cell bodies and on membranes of oligodendrocytes but not along myelin sheaths.[10,11,29] Moreover, *KIR4.1*$^{-/-}$ mice were shown to have lost inwardly rectifying K$^+$ currents on oligodendrocytes, indicating that Kir4.1 is located on cell membranes.[9,12] Notably, KIR4.1 does not seem to be expressed in Schwann cells.[41] Besides oligodendrocytes, KIR4.1 homotetramer channels are highly expressed in perivascular astrocytes and astrocytic endfeet that play a key role in siphoning potassium into the lumen of capillaries.[13,42]

FIGURE 6: Chronic inactive demyelinated white matter (WM) lesions. (A) Myelin oligodendrocyte glycoprotein (MOG) immunohistochemistry (IHC; Luxol fast blue/Periodic acid-Schiff [LFB-PAS] staining shows section overview with chronic inactive demyelinated WM lesion framed). (B) Major histocompatibility complex (MHC)-II IHC of same lesion in A showing little MHC-II$^+$ microglia activation (*right inset* demonstrates in higher magnification MHC-II$^+$ microglia *[cyan arrowheads]*). (C) KIR4.1 and (D) glial fibrillary acidic protein (GFAP) immunoreactivity (IR) of the same lesion area shown in A and B demonstrates an enhanced KIR4.1 IR paralleled by GFAP IR in demyelinated WM (DMWM). (E–H) Lesion overview shows normal-appearing WM (NAWM), periplaque WM (PPWM), and DMWM lesion areas by double staining for KIR4.1 (red, F), and MOG (green, G). (I) KIR4.1 and (J) GFAP IR of framed lesion area in C and D demonstrates in higher magnification regained and increased KIR4.1 (I) IR paralleled by increased GFAP (J) IR in DMWM. (K, L) Summary of astroglial KIR4.1 and GFAP IR in chronic inactive lesions. Graphs show enhanced astroglial KIR4.1 and GFAP IR in 12 (n = 11 for GFAP) DMWM (K) and 17 PPWM (L) lesion areas (x-axis: 0 = loss of IR, − = less than control level IR; −/+ = control level IR, + = more than control level IR, ++ = strongly enhanced IR; y-axis: number of multiple sclerosis [MS] lesion areas). Note regaining of KIR4.1 IR in DMWM. (M–O) Regaining of KIR4.1 IR (red, N) in chronic inactive demyelinated MS lesion paralleled by astroglial GFAP IR (green, O); note enhanced KIR4.1 IR in PPWM area. (P–S) Enhanced astroglial KIR4.1 IR (red, Q; *white arrows*) in chronic inactive DMWM with few preserved cyclic nucleotide phosphodiesterase (CNPase)$^+$ (green, R) myelin sheaths (*white arrowheads;* magnification: A–D, I, J, ×50; E–H, M–O, ×10; P–S, ×400; scale bars: D, M, 200μm; E, 500μm; J, 100μm; P, 20μm). DAPI = 4′,6-diamidino-2-phenylindole.

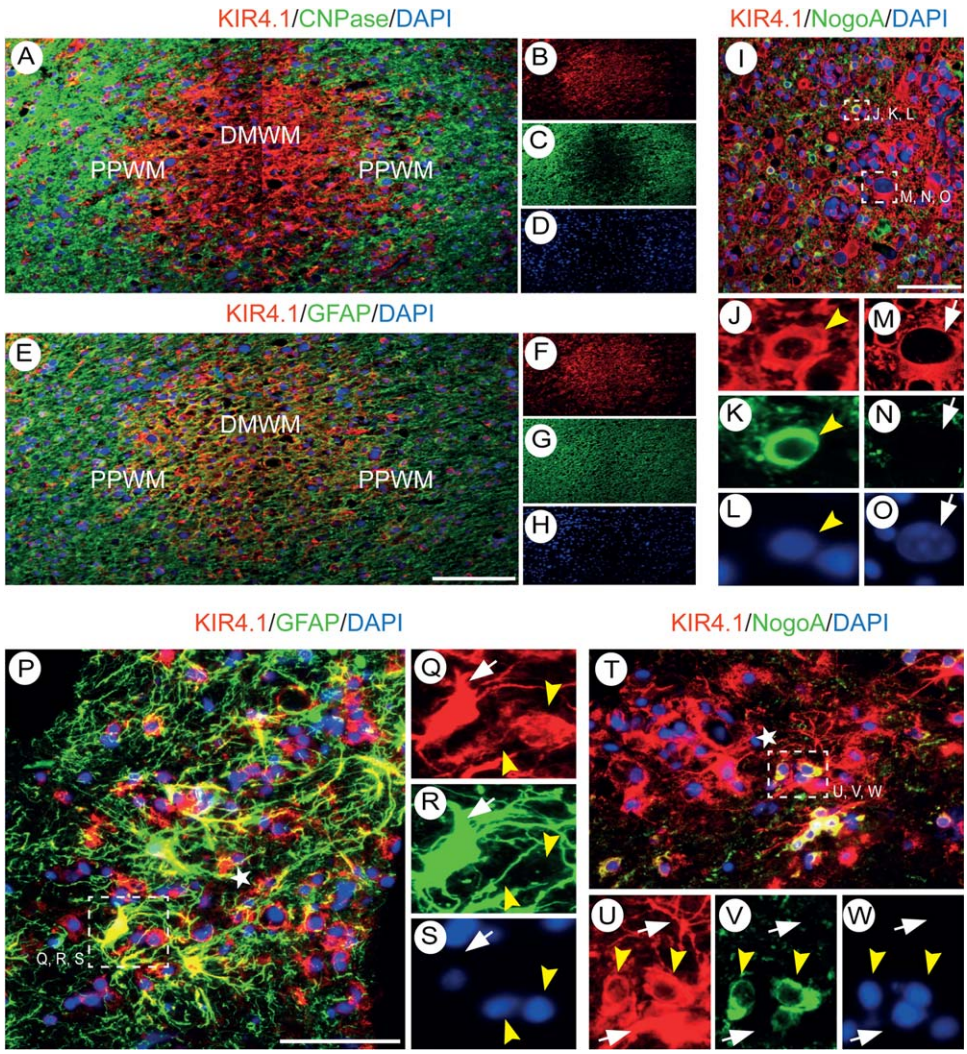

FIGURE 8: KIR4.1 immunoreactivity in progressive multifocal leukoencephalopathy (PML) and acute disseminated encephalomyelitis (ADEM) lesions. (A–D) Enhanced KIR4.1 immunoreactivity (IR; red, B) in demyelinated white matter (DMWM) area of a PML lesion; note the loss of cyclic nucleotide phosphodiesterase (CNPase) IR in DMWM (green, C). (E–H) Enhanced IR for KIR4.1 (red, F) is paralleled by glial fibrillary acidic protein (GFAP) IR (green, G) in PML DMWM. (I–O) KIR4.1 (red, J and M) is upregulated in enlarged and presumably JC virus–infected oligodendrocytes (J–L) and astrocytes in PML lesions (M–O). (P–S) Perivascular ADEM lesion with enhanced KIR4.1 IR (red, Q) in reactive GFAP$^+$ astrocytes (green, R, *white arrow*) with some preserved KIR4.1$^+$ oligodendrocytes (red, Q, *yellow arrowheads*) in the periplaque white matter (PPWM). (T–W) Preserved or new NogoA$^+$ (green, V, *yellow arrowheads*) oligodendrocytes are KIR4.1$^+$ (red, U, *yellow arrowheads*) in ADEM lesion (white arrows mark astrocytes; original magnification: A–W, ×200; scale bars: E, I, P, 100μm). DAPI = 4′,6-diamidino-2-phenylindole.

Concerning MS lesion pathology, we observed a preferential loss of KIR4.1 IR on oligodendrocytes and perivascular astrocytes in acute demyelinating and chronic active demyelinated MS lesions. Whereas oligodendrocytes were generally lost in DMWM areas, we noted a differential loss of KIR4.1 IR on a subset of otherwise preserved oligodendrocytes (NogoA$^+$/MOG$^+$) in PPWM areas of early lesions. In DMWM areas of acute and chronic active lesions, astroglial IR was decreased for KIR4.1 but sustained for GFAP. Reactive astrocytic cell bodies at lesion edges of acute and chronic active lesions were KIR4.1$^+$ and KIR5.1$^+$, suggesting formation of both homo- and heterotetrameric KIR4.1 complexes. We also found evidence for complement activation and KIR4.1-related phagocytosis and apoptosis in CSF KIR4.1-IgG$^+$ patients. Although we were able to isolate KIR4.1-IgG from single MS lesions from CSF KIR4.1-IgG$^+$ patients, it remains unclear whether these antibodies are involved in the activation of the complement cascade.

In both inactive chronic demyelinated and remyelinating MS lesions, we observed a regaining of KIR4.1 IR. This was due to a widespread upregulation of KIR4.1 along astrocytic fibers in demyelinated areas and KIR4.1 expression in presumably new myelinating oligodendrocytes in RMWM areas.[9,43] Comparing KIR4.1 IR

patterns in other neuropathological lesions (PML, ADEM, and glioma tissue), we did not observe a similar differential and stage-dependent loss of KIR4.1 IR on glial cells as seen in MS lesions.

Overall, a specific autoimmune response against KIR4.1 would be compatible with the pathological findings observed in our study. The demyelinating process in MS usually starts around small vessels where homotetrameric KIR4.1 is expressed at high levels. Binding of autoantibodies to the channel may lead to Fc-receptor–mediated complement and macrophage activation and subsequent death of those cells that express high levels of KIR4.1 homotetramers, respectively.

Moreover, binding of antibodies to KIR4.1 might result in internalization of KIR4.1 complexes, possibly explaining the differential loss of KIR4.1 IR on a subset of oligodendrocytes at the borders and of astrocytes in the center of acute and chronic active MS lesions.[44,45]

Functional inactivation of KIR4.1 might interfere with potassium siphoning by astrocytes, resulting in impaired potassium and water homeostasis.[46] Moreover, the expression of KIR4.1 in oligodendrocytes and the association with $Cx47^+$ gap junctions suggest that the channel plays an important role for potassium exchange between oligodendrocytes and astrocytes.[29] In particular, these gap junctions seem to be disturbed in MS lesions.[42,47,48] Consecutively, a breakdown of the glial interface would interfere with potassium buffering, leading to increased extracellular and potentially excitotoxic potassium levels.[42,46]

Notably, molecules such as KIR4.1 and AQP4 are downregulated in response to nonspecific tissue damage as seen in the sclerotic hippocampus from epilepsy patients.[49] Similarly, downregulation of astrocytic KIR4.1 and AQP4 and disturbed KIR4.1-mediated K^+ buffering were reported in models of Huntington disease and amyotrophic lateral sclerosis and observed following spinal cord injury, optic nerve crush, and CNS ischemia.[50–54] However, these changes do not seem to be primarily focused on perivascular astrocytes and oligodendrocytes (as in the case of homotetrameric KIR4.1), nor do they go along with an antibody response to these antigens.[7] Of note, we did not examine KIR4.1 IR in NMO lesions. However, as KIR4.1 is strongly expressed in perivascular astrocytes and localized in astroglial endfeet, one might expect a partial loss of astrocytic KIR4.1 IR in NMO lesions, which is in line with previous reports on astrocytic damage in MS lesions.[55,56] However, it is unclear how circulating antibodies can cross the endothelial barrier, get access to the perivascular space, and start the inflammatory cascade. Likewise, APQ4-specific antibodies from NMO patients transferred into mice are inert if they are administered into the periphery but are highly pathogenic if they are injected into the CNS compartment.[57,58] KIR4.1 as well as AQP4 antibodies belong to the IgG_1 and IgG_3 subtypes, suggesting that their generation requires the help of antigen-specific T cells, and these T cells might open up the blood–brain barrier and contribute to the inflammatory process.[7,57,58]

In the current study, we characterized the expression profile of KIR4.1 in glial cells in the normal human brain. Moreover, we described a differential and stage-dependent loss of KIR4.1 IR in MS lesions. Given the differential expression profile of KIR4.1 in glial cells, our findings would suggest that if an KIR4.1-specific antibody contributes to tissue damage in MS lesions, this antibody should target homotetrameric KIR4.1 channels rather than heterotetrameric KIR4.1/5.1 channels. However, histopathologic analyses can only provide circumstantial evidence, and definite proof for this hypothesis will only be possible through interventional studies in in vivo models using laboratory animals. Thus, further clinical and experimental studies are necessary to strengthen the hypothesis that KIR4.1 is a primary target of the immune response in MS.

Acknowledgment

L.S. was supported by a Du Pré Travel Grant of the Multiple Sclerosis International Federation and intramural funding of the medical faculty of the Technische Universität München. B.H., T.Ko., and T.Ku. were supported by grants from the German Research Foundation (SFB-TR128 Project A4, KO2964/3-2) and the German Ministry for Education and Research (German Competence Network Multiple Sclerosis, Control-MS, 01GI0917).

The C9neo antibody was kindly provided by P. Morgan, Cardiff University. The NogoA antibody was kindly provided by M. Schwab, University of Zurich.

We thank D. Gveric from the UK Multiple Sclerosis Tissue Bank for providing MS and control tissue samples; and V. Grummel, C. Nowak, Y. Schäfer, J. Steele, and I. Höpner for skillful technical assistance.

Potential Conflicts of Interest

L.S.: grants, Genzyme. R.S.: patent, Detection of antibodies against KIR4.1 in a subpopulation of MS patients. T.Ku.: speaking fees, Novartis, Teva. B.H.: grants, Hoffman-La Roche; patent, Detection of antibodies against KIR4.1 in a subpopulation of MS patients.

References

1. Krumbholz M, Derfuss T, Hohlfeld R, Meinl E. B cells and antibodies in multiple sclerosis pathogenesis and therapy. Nat Rev Neurol 2012;8:613–623.

2. McLaughlin KA, Wucherpfennig KW. B cells and autoantibodies in the pathogenesis of multiple sclerosis and related inflammatory demyelinating diseases. Adv Immunol 2008;98:121–149.
3. Schirmer L, Srivastava R, Hemmer B. To look for a needle in a haystack: the search for autoantibodies in multiple sclerosis. Mult Scler 2014;20:271–279.
4. Barnett MH, Prineas JW. Relapsing and remitting multiple sclerosis: pathology of the newly forming lesion. Ann Neurol 2004;55: 458–468.
5. Frohman EM, Racke MK, Raine CS. Multiple sclerosis—the plaque and its pathogenesis. N Engl J Med 2006;354:942–955.
6. Lassmann H, Bruck W, Lucchinetti CF. The immunopathology of multiple sclerosis: an overview. Brain Pathol 2007;17:210–218.
7. Srivastava R, Aslam M, Kalluri SR, et al. Potassium channel KIR4.1 as an immune target in multiple sclerosis. N Engl J Med 2012; 367:115–123.
8. Takumi T, Ishii T, Horio Y, et al. A novel ATP-dependent inward rectifier potassium channel expressed predominantly in glial cells. J Biol Chem 1995;270:16339–16346.
9. Neusch C, Rozengurt N, Jacobs RE, et al. Kir4.1 potassium channel subunit is crucial for oligodendrocyte development and in vivo myelination. J Neurosci 2001;21:5429–5438.
10. Kalsi AS, Greenwood K, Wilkin G, Butt AM. Kir4.1 expression by astrocytes and oligodendrocytes in CNS white matter: a developmental study in the rat optic nerve. J Anat 2004;204:475–485.
11. Poopalasundaram S, Knott C, Shamotienko OG, et al. Glial heterogeneity in expression of the inwardly rectifying K(+) channel, Kir4.1, in adult rat CNS. Glia 2000;30:362–372.
12. Djukic B, Casper KB, Philpot BD, et al. Conditional knock-out of Kir4.1 leads to glial membrane depolarization, inhibition of potassium and glutamate uptake, and enhanced short-term synaptic potentiation. J Neurosci 2007;27:11354–11365.
13. Ishii M, Fujita A, Iwai K, et al. Differential expression and distribution of Kir5.1 and Kir4.1 inwardly rectifying K+ channels in retina. Am J Physiol Cell Physiol 2003;285:C260–C267.
14. Higashi K, Fujita A, Inanobe A, et al. An inwardly rectifying K(+) channel, Kir4.1, expressed in astrocytes surrounds synapses and blood vessels in brain. Am J Physiol Cell Physiol 2001;281:C922–C931.
15. Tang X, Taniguchi K, Kofuji P. Heterogeneity of Kir4.1 channel expression in glia revealed by mouse transgenesis. Glia 2009;57: 1706–1715.
16. Hibino H, Fujita A, Iwai K, et al. Differential assembly of inwardly rectifying K+ channel subunits, Kir4.1 and Kir5.1, in brain astrocytes. J Biol Chem 2004;279:44065–44073.
17. Tanemoto M, Kittaka N, Inanobe A, Kurachi Y. In vivo formation of a proton-sensitive K+ channel by heteromeric subunit assembly of Kir5.1 with Kir4.1. J Physiol 2000;525(pt 3):587–592.
18. Bockenhauer D, Feather S, Stanescu HC, et al. Epilepsy, ataxia, sensorineural deafness, tubulopathy, and KCNJ10 mutations. N Engl J Med 2009;360:1960–1970.
19. Lucchinetti C, Bruck W, Parisi J, et al. Heterogeneity of multiple sclerosis lesions: implications for the pathogenesis of demyelination. Ann Neurol 2000;47:707–717.
20. Lassmann H. Review: The architecture of inflammatory demyelinating lesions: implications for studies on pathogenesis. Neuropathol Appl Neurobiol 2011;37:698–710.
21. Magliozzi R, Howell O, Vora A, et al. Meningeal B-cell follicles in secondary progressive multiple sclerosis associate with early onset of disease and severe cortical pathology. Brain 2007;130(pt 4):1089–1104.
22. Lucchinetti CF, Mandler RN, McGavern D, et al. A role for humoral mechanisms in the pathogenesis of Devic's neuromyelitis optica. Brain 2002;125(pt 7):1450–1461.
23. Lennon VA, Wingerchuk DM, Kryzer TJ, et al. A serum autoantibody marker of neuromyelitis optica: distinction from multiple sclerosis. Lancet 2004;364:2106–2112.
24. Roemer SF, Parisi JE, Lennon VA, et al. Pattern-specific loss of aquaporin-4 immunoreactivity distinguishes neuromyelitis optica from multiple sclerosis. Brain 2007;130(pt 5):1194–1205.
25. Misu T, Fujihara K, Kakita A, et al. Loss of aquaporin 4 in lesions of neuromyelitis optica: distinction from multiple sclerosis. Brain 2007;130(pt 5):1224–1234.
26. Kraus V, Srivastava R, Kalluri SR, et al. Potassium channel KIR4.1-specific antibodies in children with acquired demyelinating CNS disease. Neurology 2014;82:470–473.
27. O'Connor KC, Appel H, Bregoli L, et al. Antibodies from inflamed central nervous system tissue recognize myelin oligodendrocyte glycoprotein. J Immunol 2005;175:1974–1982.
28. Kuhlmann T, Remington L, Maruschak B, et al. Nogo-A is a reliable oligodendroglial marker in adult human and mouse CNS and in demyelinated lesions. J Neuropathol Exp Neurol 2007;66:238–246.
29. Menichella DM, Majdan M, Awatramani R, et al. Genetic and physiological evidence that oligodendrocyte gap junctions contribute to spatial buffering of potassium released during neuronal activity. J Neurosci 2006;26:10984–10991.
30. Butt AM, Kalsi A. Inwardly rectifying potassium channels (Kir) in central nervous system glia: a special role for Kir4.1 in glial functions. J Cell Mol Med 2006;10:33–44.
31. Bruck W, Porada P, Poser S, et al. Monocyte/macrophage differentiation in early multiple sclerosis lesions. Ann Neurol 1995;38: 788–796.
32. Han MH, Hwang SI, Roy DB, et al. Proteomic analysis of active multiple sclerosis lesions reveals therapeutic targets. Nature 2008; 451:1076–1081.
33. Schirmer L, Albert M, Buss A, et al. Substantial early, but nonprogressive neuronal loss in multiple sclerosis (MS) spinal cord. Ann Neurol 2009;66:698–704.
34. Barnett MH, Parratt JD, Cho ES, Prineas JW. Immunoglobulins and complement in postmortem multiple sclerosis tissue. Ann Neurol 2009;65:32–46.
35. Prineas JW, Parratt JD. Oligodendrocytes and the early multiple sclerosis lesion. Ann Neurol 2012;72:18–31.
36. Gheuens S, Wuthrich C, Koralnik IJ. Progressive multifocal leukoencephalopathy: why gray and white matter. Annu Rev Pathol 2013;8:189–215.
37. Berger JR, Aksamit AJ, Clifford DB, et al. PML diagnostic criteria: consensus statement from the AAN Neuroinfectious Disease Section. Neurology 2013;80:1430–1438.
38. Young NP, Weinshenker BG, Parisi JE, et al. Perivenous demyelination: association with clinically defined acute disseminated encephalomyelitis and comparison with pathologically confirmed multiple sclerosis. Brain 2010;133(pt 2):333–348.
39. Warth A, Mittelbronn M, Wolburg H. Redistribution of the water channel protein aquaporin-4 and the K+ channel protein Kir4.1 differs in low- and high-grade human brain tumors. Acta Neuropathol 2005;109:418–426.
40. Lucchinetti CF, Guo Y, Popescu BF, et al. The pathology of an autoimmune astrocytopathy: lessons learned from neuromyelitis optica. Brain Pathol 2014;24:83–97.
41. Vit JP, Ohara PT, Bhargava A, et al. Silencing the Kir4.1 potassium channel subunit in satellite glial cells of the rat trigeminal ganglion results in pain-like behavior in the absence of nerve injury. J Neurosci 2008;28:4161–4171.
42. Rash JE. Molecular disruptions of the panglial syncytium block potassium siphoning and axonal saltatory conduction: pertinence to neuromyelitis optica and other demyelinating diseases of the central nervous system. Neuroscience 2010;168:982–1008.

43. Kuhlmann T, Miron V, Cui Q, et al. Differentiation block of oligodendroglial progenitor cells as a cause for remyelination failure in chronic multiple sclerosis. Brain 2008;131(pt 7):1749–1758.

44. Hinson SR, Roemer SF, Lucchinetti CF, et al. Aquaporin-4-binding autoantibodies in patients with neuromyelitis optica impair glutamate transport by down-regulating EAAT2. J Exp Med 2008;205:2473–2481.

45. Hughes EG, Peng X, Gleichman AJ, et al. Cellular and synaptic mechanisms of anti-NMDA receptor encephalitis. J Neurosci 2010;30:5866–5875.

46. Chever O, Djukic B, McCarthy KD, Amzica F. Implication of Kir4.1 channel in excess potassium clearance: an in vivo study on anesthetized glial-conditional Kir4.1 knock-out mice. J Neurosci 2010;30:15769–15777.

47. Kamasawa N, Sik A, Morita M, et al. Connexin-47 and connexin-32 in gap junctions of oligodendrocyte somata, myelin sheaths, paranodal loops and Schmidt-Lanterman incisures: implications for ionic homeostasis and potassium siphoning. Neuroscience 2005;136:65–86.

48. Markoullis K, Sargiannidou I, Schiza N, et al. Gap junction pathology in multiple sclerosis lesions and normal-appearing white matter. Acta Neuropathol 2012;123:873–886.

49. Heuser K, Eid T, Lauritzen F, et al. Loss of perivascular Kir4.1 potassium channels in the sclerotic hippocampus of patients with mesial temporal lobe epilepsy. J Neuropathol Exp Neurol 2012;71:814–825.

50. Tong X, Ao Y, Faas GC, et al. Astrocyte Kir4.1 ion channel deficits contribute to neuronal dysfunction in Huntington's disease model mice. Nat Neurosci 2014;17:694–703.

51. Kaiser M, Maletzki I, Hulsmann S, et al. Progressive loss of a glial potassium channel (KCNJ10) in the spinal cord of the SOD1 (G93A) transgenic mouse model of amyotrophic lateral sclerosis. J Neurochem 2006;99:900–912.

52. Olsen ML, Campbell SC, McFerrin MB, et al. Spinal cord injury causes a wide-spread, persistent loss of Kir4.1 and glutamate transporter 1: benefit of 17 beta-oestradiol treatment. Brain 2010;133(pt 4):1013–1025.

53. Dibas A, Oku H, Fukuhara M, et al. Changes in ocular aquaporin expression following optic nerve crush. Mol Vis 2010;16:330–340.

54. Wang YF, Gu YT, Xu WB, Lv G. Temporary loss of perivascular aquaporin-4 in white matter after the spinal cord ischemic injury of rats. Neuroreport 2009;20:145–149.

55. Parratt JD, Prineas JW. Neuromyelitis optica: a demyelinating disease characterized by acute destruction and regeneration of perivascular astrocytes. Mult Scler 2010;16:1156–1172.

56. Brosnan CF, Raine CS. The astrocyte in multiple sclerosis revisited. Glia 2013;61:453–465.

57. Bradl M, Misu T, Takahashi T, et al. Neuromyelitis optica: pathogenicity of patient immunoglobulin in vivo. Ann Neurol 2009;66:630–643.

58. Bennett JL, Lam C, Kalluri SR, et al. Intrathecal pathogenic anti-aquaporin-4 antibodies in early neuromyelitis optica. Ann Neurol 2009;66:617–629.